Renewable Energy 244 (2025) 122622

Contents lists available at ScienceDirect

Renewable Energy

journal homepage: www.elsevier.com/locate/renene

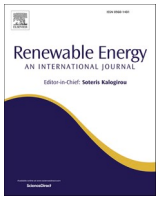

A novel radiative cooling system with a dissimilar material-based compound parabolic concentrator for mitigating daytime solar radiation impact

Ya Dan [a], Qiliang Wang [a,*], Mingke Hu [b], Dongliang Zhao [c], Gang Pei [d], Yuehong Su [a,**], Saffa Riffat [a]

[a] Department of Architecture and Built Environment, The University of Nottingham, Nottingham, NG7 2RD, United Kingdom
[b] School of Electrical Engineering, Southwest Jiaotong University, Chengdu, 610031, China
[c] School of Energy and Environment, Southeast University, Nanjing, Jiangsu, 210096, China
[d] Department of Thermal Science and Energy Engineering, University of Science and Technology of China, Hefei, 230026, China

ARTICLE INFO

Keywords:
Radiative cooling
Compound parabolic concentrator
Transparent infrared-reflective coating
Building
Solar profile angle

ABSTRACT

Radiative sky cooling (RC) is a promising passive heat dissipation technology for building energy conservation but suffers from sensitivity to daytime solar radiation and an inherently low cooling power density. To address these challenges, a novel dissimilar material-based compound parabolic concentrator (DCPC) is first proposed and integrated into an RC system. The asymmetric DCPC features a dissimilar material design: a transparent wing framework covered with a transparent infrared-reflective film (TIRF) on one side and a high-reflectivity mirror wing on the other, aiming to enhance solar shielding while maximizing thermal emission for RC panels. In this work, a mathematical model, validated through experiments conducted in Nottingham, UK, is developed to explore the effects of TIRF's optical properties and the module's tilt angle on cooling performance. Effects of diverse tilt angles for the DCPC-RC module are also analysed based on annual solar profile angles. The experiment results demonstrate that the DCPC-RC module's emitter can achieve sub-ambient temperature during the daytime. When located in Rome and tilted at 30° toward the anti-sunward side, it achieves an average cooling power density of 135.24 W/m^2 within the solar profile angles of 40–50°, a 22.7 % increase over the horizontal module. This work establishes the DCPC-RC system as an efficient and scalable solution for enhancing passive cooling performance in energy-efficient buildings across diverse climatic conditions.

1. Introduction

The ever-increasing demands for heating and cooling in modern buildings result in massive energy consumption [1,2]. However, concerns about energy shortages and environmental damages have escalated because 81 % of the world's primary energy supply is still non-renewable and environmentally unfriendly energy sources (such as fossil fuels) [3,4]. Therefore, ensuring the sustainable development of society and advancing research into renewable energy technologies are viewed as critically important [5,6]. Among them, radiative sky cooling (RC) technology has attracted significant attention for its capability to passively emit the Earth's waste heat into the cold outer space through a transparent 'atmospheric window' with a wavelength of 8–13 μm [7,8]. Its potential for self-cooling without the need for additional energy input makes it enormously promising for building cooling applications [9–11]. However, the inherently low power density of RC technology, typically characterized by a cooling flux of approximately 100 W/m^2 [12] at ambient temperature, is easily offset by the intense power density of daytime solar radiation, approximately 1000 W/m^2 [13,14]. This disparity makes RC technology inadequate for meeting the all-day cooling needs of buildings, particularly during the daytime when cooling demands are highest [15]. Therefore, it is crucial to enhance the cooling power density and reduce the impact of solar radiation on the RC system.

This article is part of a special issue entitled: AESMT'24_RENE published in Renewable Energy.

* Corresponding author.
** Corresponding author.
E-mail addresses: qiliang.wang1@nottingham.ac.uk (Q. Wang), yuehong.su@nottingham.ac.uk (Y. Su).

https://doi.org/10.1016/j.renene.2025.122622
Received 7 September 2024; Received in revised form 28 December 2024; Accepted 5 February 2025
Available online 10 February 2025

The mainstream focus of current research is to improve the cooling performance of RC systems by developing RC emitter materials with near-ideal spectral selectivity. These materials are characterized by extremely low absorptivity in the solar spectrum and high emissivity close to 1 within the 'atmospheric window' [16,17]. As research progresses, many near-ideal spectrally selective materials have been developed, verifying the feasibility of achieving RC throughout the day [17–19]. However, the production of these materials with superior properties necessitates complex and rigorous processing methods [20–22], which makes them costly and hinders their large-scale application in actual building scenarios. Fortunately, beyond utilizing spectrally selective materials to minimize solar radiation absorption, RC systems can also improve cooling power by incorporating shading devices to block solar radiation. Common shading devices for RC systems fall into two categories. The first type includes enclosed structures on four sides, such as truncated cone shields [23], mirror cone shields [24] and parabolic reflective dish shields [25]. The second type involves unenclosed structures, such as flat plate shields [24] and ring shields [8, 26]. These shading devices have been experimentally proven to effectively block most incident sunlight from the RC system. However, these independently installed shading devices often require significant space and may introduce new challenges concerning installation and aesthetic compatibility in real-world applications, particularly when integrated with buildings.

In addition to installing independent shading devices around the RC systems, recently proposed concentrated RC systems [27–30] show the potential to address both challenges simultaneously. The concentrated RC systems can be viewed as replacing the solar collector at the bottom of the concentrator with a flat RC emitter, enabling easy integration with building roofs or other envelopes. Furthermore, the height difference between the concentrator and the RC emitter allows it to effectively block sunlight at specific times. Inspired by advancements in RC systems, the compound parabolic concentrator-based RC (CPC-RC) module was developed [31]. To investigate the impact of this innovative structure on the enhancement of RC performance, comparative experiments were conducted by our team. It was revealed by nighttime experiments that the cooling performance of the CPC-RC module is 30 % greater than that of the flat emitters without concentrators [32]. This is because the unique CPC structure can concentrate the emitted thermal radiation from the emitter towards the almost transparent zenith and uses the height difference between the CPC and the emitter as a shielding mechanism to block unfavourable thermal radiation from the side surroundings, thereby improving cooling capacity. However, during the daytime, when the solar incident angle is less than the maximum half-acceptance angle (θ_{max}) of the CPC, its concentrating ability causes the module to absorb more solar radiation, particularly at noon [33]. Additionally, the configuration of the CPC-RC module lacks extra space for solar energy utilization [34], preventing it from generating other forms of energy and causing a loss of solar resources. This limitation reduces its functional flexibility and year-round adaptability for various applications.

In this study, a novel RC module based on CPC with dissimilar materials (termed DCPC-RC module) is proposed to address the challenges of intense solar radiation on RC and the waste of solar radiation resources. This paper first demonstrates the exceptional all-day cooling capability of the DCPC-RC module through field experiments. Additionally, utilizes preliminary numerical studies [35] to accurately characterize its net cooling power density, showcasing its effectiveness in mitigating the impact of solar radiation. Furthermore, the paper investigates the effects of various parameters, including the DCPC wing frameworks with different spectral splitting films and varying module tilt angles, on the cooling performance of the DCPC-RC module. The development of this innovative RC module offers new insights for the broader application of radiative cooling technology, highlighting its significant potential to enhance cooling efficiency and environmental adaptability.

2. Description of the DCPC-RC system

In this section, the configuration and features of the proposed DCPC-RC module will be introduced in detail, focusing on its functional advantages compared to the conventional mirror CPC-RC. Additionally, the test rig established in Nottingham for validation will be presented.

2.1. Introduction of DCPC-RC module and its cooling performance advantages

As illustrated in Fig. 1, the DCPC-RC multi-module system comprises multiple identical DCPC-RC modules, with each module's side openings facing east-west. Within each DCPC-RC module, the DCPC wing frameworks are made of two different materials: the north-facing side features a transparent wing framework covered with a transparent infrared-reflective film (TIRF), which allows sunlight to pass through while reflecting infrared thermal radiation, while the south-facing side is a standard specular metal wing framework. The RC emitters are located at the bottom of the DCPC structures. Two adjacent modules are interconnected by their wing frameworks. Each module in the system features an aperture width of 40 mm and an emitter width of 20 mm. And the module's height and length are 40 and 200 mm, respectively.

Compared to the DCPC-RC multi-module system, a typical mirror CPC-RC multi-module system leaves the space between adjacent module wing frameworks underutilized, with only the bottom of the CPC serving as the effective cooling area, leading to low utilization efficiency. Furthermore, due to the concentrating properties of the mirror CPC, more solar radiation is concentrated on the RC emitter when the solar incident angle is smaller than the θ_{max} of the CPC, negatively affecting the RC performance. However, in the DCPC-RC multi-module system, the yellow middle area (as shown in Fig. 1) created by the wing frameworks of adjacent modules can function as a solar collector, absorbing sunlight passing through the transparent side of the module. This configuration demonstrates the potential of this system to obtain cooling power and solar energy collection simultaneously. Nevertheless, the primary focus of this paper is not on the utilization of solar energy by the system but rather on its impact on RC performance. Therefore, the utilization of the solar collector will not be involved in this study.

Fig. 2 shows the radiative heat exchange between (a) the mirror CPC-RC module and (b) the DCPC-RC system and the surroundings. It can be seen that the traditional CPC with opaque mirror wing frameworks on both sides concentrates solar radiation, whose incident angle falls within the CPC's θ_{max} range, onto the RC emitter. This concentration typically weakens the cooling performance of the module during the daytime. In contrast, the transparent side of the DCPC structure allows solar radiation to pass through it to the collectors on the sides, thereby reducing its

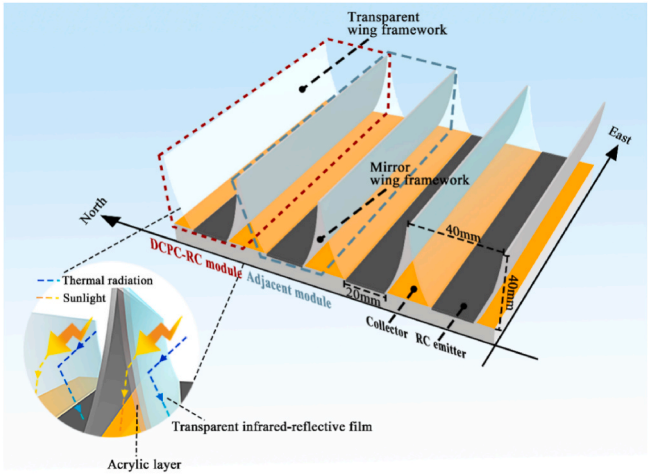

Fig. 1. Schematic diagram of DCPC-RC multi-module system.

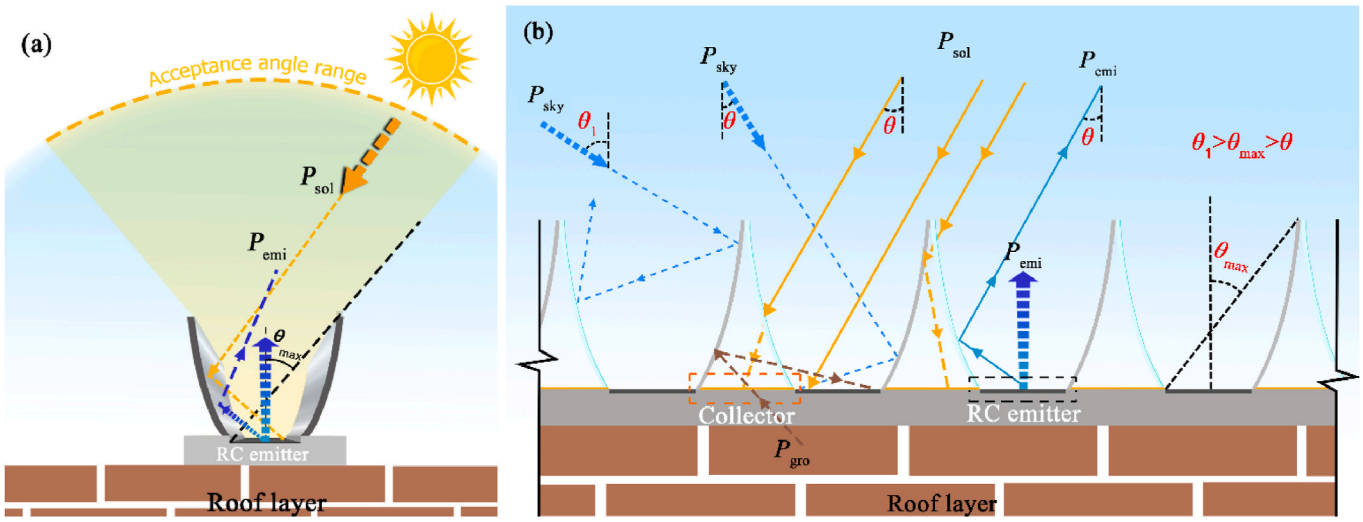

Fig. 2. Radiative heat exchange between (a) mirror CPC-RC and (b) DCPC-RC system and external environment.

impact on the RC emitter. Moreover, since the transparent wing framework covered with TIRF exhibits high reflectivity under the 'atmospheric window', the DCPC can concentrate the thermal radiation emitted by the RC emitter to a smaller range of zenith angles, similar to the mirror CPC. Finally, both structures can shield the unfavourable radiation from the sky and the sun whose incident angle exceeds the θ_{max} of CPC and DCPC, preventing it from reaching the RC emitter. Therefore, theoretically, DCPC-RC system's configuration enhances the cooling efficiency by reducing unwanted thermal gain during the day while maximizing cooling power under favourable conditions.

2.2. Experiment rigs

This section introduces the different RC modules and measuring rigs in the field experiment in Nottingham (52.94 °N, 1.09 °W), UK, as shown in Fig. 3. The whole experimental system is composed of several key components, including three RC modules, which are DCPC-RC, mirror CPC-RC, and flat-RC modules, K-type thermocouples, a data logger, a pyranometer, a weather station, a thermocouple shelter and a laptop. The pyranometer is used to measure the total solar irradiance of the plane where the modules are located. Meanwhile, the weather station obtains real-time weather parameters such as wind speed and relative humidity. Several K-type thermocouples are attached to the bottom of the RC emitters of different modules to measure the temperature of the emitter. The ambient temperature is measured by a thermocouple in the shelter at the same height as the module. All the measured data is collected by the data logger and summarized in the laptop. Furthermore, to minimize convective and conductive heat transfer between the RC emitter and ambient air, a 15 μm thick polyethylene (PE) film is positioned 5 mm above the emitter. The detailed spectral properties of the experimental materials are listed in Table 1, while Table 2 provides the test and monitoring equipment along with their associated

Table 1
Spectral properties of materials in the experimental system (spectral characteristics are weighted average values).

Parameter	Description	Value
τ_{TIRF}	Solar transmittance of TIRF	0.856 [36]
ρ_{TIRF}	Infrared reflectivity of transparent wing framework	0.50 [36]
τ_{TCPC}	Solar transmittance of transparent wing framework	0.90 [37]
τ_{PE}	Solar transmittance of PE film	0.90 [32]
ε_{emi}	Infrared emissivity of RC emitter	0.94 [1]
α_{emi}	Solar absorptivity of RC emitter	0.134 [1]
ρ_{MCPC}	Infrared reflectivity of mirror wing framework	0.95 [32]

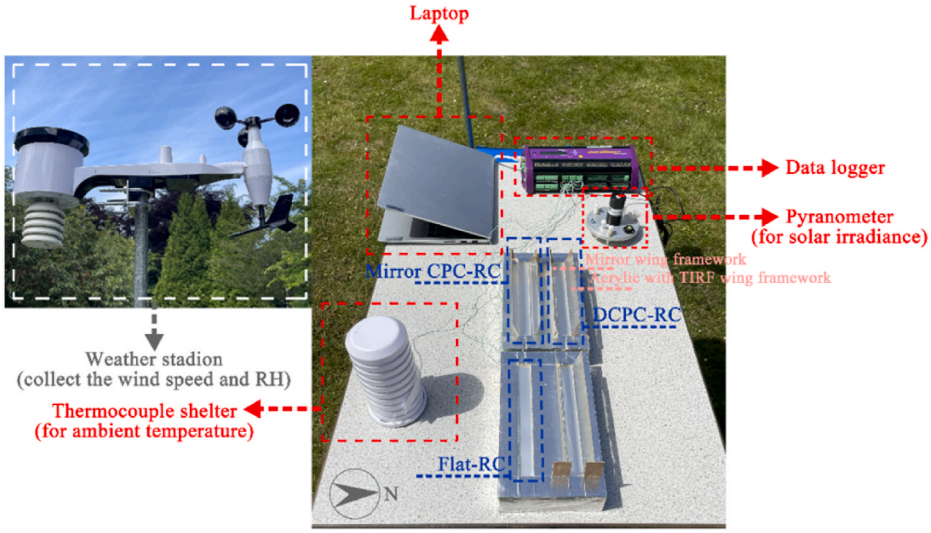

Fig. 3. In-situ experimental setup of the RC systems.

Table 2
List of testing and monitoring devices in the experimental system.

Device	Specification	Uncertainty
Data logger	Data Taker DT85	/
Pyranometer	SKL 2650	±2 %
Thermocouples	K-type	±0.05 °C
Weather station for wind speed	CE-FWS 20N-2	±1 m/s
Weather station for relative humidity	CE-FWS 20N-2	±4 % within 20–80 %

uncertainties.

3. Methodology

In this section, the mathematical model characterizing the net radiative cooling power for the RC modules is first introduced. Given that the complete mathematical framework has been thoroughly explained in our previous studies [33,35], only the key equations are presented in this paper, with appropriate references to Refs. [33,35]. Additionally, the software and approaches used in the simulation are briefly described, and the accuracy of the model is verified using experimental data. Finally, the definition and calculation method of the solar profile angle are provided.

3.1. Mathematical model

In the modelling approach, the net radiative cooling power density (P_{cool}) obtained by the DCPC-RC module can be expressed as [12,38]:

$$P_{cool} = P_{emi} - P_{sky} - P_{sol} - P_{non-rad} \tag{1}$$

where P_{emi} is the thermal radiation power density of the RC emitter, W/m^2; P_{sky} is the emitter-absorbed thermal radiation power density of the sky, W/m^2, W/m^2; P_{sol} is the emitter-absorbed solar irradiance, W/m^2, and $P_{non\text{-}rad}$ is the non-radiative heat exchange power density between the emitter and surroundings, W/m^2. In this paper, the RC emitter temperature (T_{emi}) is assumed to be equal to the ambient temperature (T_{amb}), allowing the neglect of $P_{non\text{-}ra}$ between the RC module and its surroundings.

Among them, the thermal radiation power of the emitter is not affected by the external environment and is only determined by its own spectral characteristics, which can be expressed as [39]:

$$P_{emi} = \varepsilon_{emi}\sigma T_{emi}^4 \tag{2}$$

where ε_{emi} is the total, hemispherical emissivity of the RC emitter; σ is Stefan-Boltzmann constant, 5.67 × 10^{-8} W m^{-2} K^{-4}; T_{emi} is the temperature of the RC emitter, °C.

The thermal radiation power from the sky absorbed by the RC emitter can be expressed as [13]:

$$P_{sky} = \int_0^{\pi/2}\int_0^{2\pi}\int_0^{\infty} \varepsilon_{sky}(\theta,\varphi,\lambda) I_b(\lambda, T_{amb}) \alpha_{emi}(\theta,\varphi,\lambda)\cos\theta \sin\theta d\lambda d\varphi d\theta \tag{3}$$

where $\varepsilon_{sky}(\theta, \varphi, \lambda)$ and $\alpha_{emi}(\theta, \varphi, \lambda)$ denote the spectral, directional emissivity and absorptivity of the sky and emitter, respectively; and $I_b(\lambda, T_{amb})$ is the blackbody spectral intensity at ambient temperature, W·m^{-2}·μm^{-1}·sr^{-1}. According to the Stefan-Boltzmann law, the P_{sky} can be expressed simplified as Eq. (4):

$$P_{sky} = \alpha_{emi}\varepsilon_{sky}\sigma T_{amb}^4 \tag{4}$$

where α_{emi} is the total, hemispherical absorptivity of the RC emitter; ε_{sky} is the total, hemispheric emissivity of the sky; T_{amb} is the temperature of the ambient, °C. Using the new modelling approach for simulation and derivation, ε_{sky} can be expressed as [35]:

$$\varepsilon_{sky} = \int_0^{\pi/2} \left[\varepsilon_{sky}(\theta)\beta_{sky}(\theta)\right] d\theta \tag{5}$$

where $\varepsilon_{sky}(\theta)$ is the equivalent emissivity of the sky in the concentric ring with a zenith angle of θ; $\beta_{sky}(\theta)$ represents the ratio of the sky radiation beam reaching the corresponding θ ring from the RC emitter to the total, hemispheric radiation beam of the RC emitter. These two parameters will be introduced in detail in Ref. [33].

In addition to the thermal radiation power of the sky, solar radiation is another important factor affecting P_{cool} during the daytime. Since the wing frameworks of DCPC in this study use different materials, they cannot concentrate sunlight during the daytime. The solar radiation absorbed by the RC emitter can be expressed as:

$$P_{sol} = \alpha_{emi}\eta_{\_sol}G_{sol} \tag{6}$$

where $\eta_{\_sol}$ is the solar receiving ratio of the DCPC; G_{sol} is the total incident solar radiation, W/m^2. Since this paper studies the different RC modules, the $\eta_{\_sol}$ for RC modules is defined as the ratio of solar radiation reaching the RC emitter to the solar radiation reaching the CPC aperture surface. The higher the $\eta_{\_sol}$, the greater the P_{sol}, which in turn negatively impacts the RC power. Therefore, this study proposes a solar shielding ratio (η) to explain the shielding effect of the CPC structure. η can be expressed as:

$$\eta = 1 - \eta_{\_sol} \tag{7}$$

3.2. Simulation model setting and validation

The modelling approach utilized in this paper first simulates the solar shielding ratio (η) of the RC modules using optical software, then determines the equivalent sky emissivity (ε_{sky}) based on the reciprocity principle, and finally employs the mathematical model to characterize the module's cooling performance. All simulated models are precisely constructed using Rhino software, with specific material properties assigned via the Rhino plug-in Photopia [40]. A detailed description of this modelling approach is introduced in Ref. [35], where the approach's accuracy is also validated using experimental results from Ref. [12]. However, as this paper introduces a novel dissimilar CPC-RC module, the accuracy and reasonableness of the modelling approach will be re-verified using experimental results by the DCPC-RC module. To validate the modelling approach, an experiment was conducted to measure the RC emitter temperatures of the mirror CPC-RC and DCPC-RC modules on the morning of 21st June and to calculate the emitter temperatures under identical environmental conditions by the mathematical model. The weather conditions on 21st of June are shown

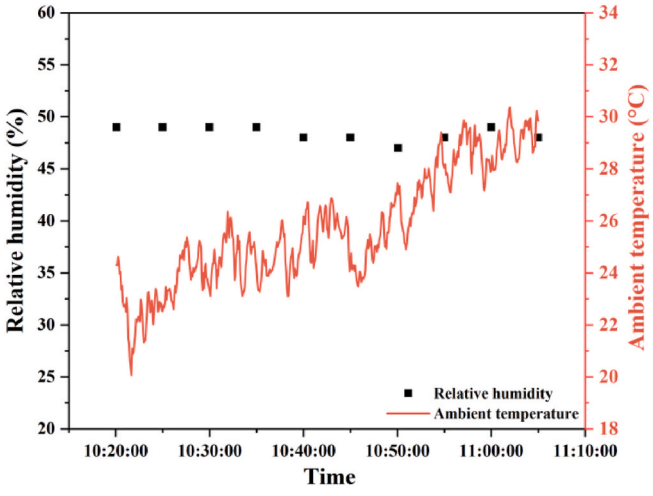

Fig. 4. Weather conditions in Nottingham, UK, on 21st June.

in Fig. 4. To quantify the discrepancy between simulated and experimental results, the root mean square deviation (*RMSD*) is employed as a metric. The formula for calculating *RMSD* is provided below [41]:

$$RMSD = \sqrt{\frac{\sum \left[\left(x_{sim} - x_{exp}\right)/x_{exp}\right]^2}{n}} \quad (8)$$

The experiment and simulated temperatures are shown in Fig. 5. The modelling approach used in this study closely aligns with experimental data. Initially, the measured emitter temperatures (T_{emi_exp}) of the mirror CPC-RC and DCPC-RC modules were 23.27 °C and 22.72 °C, respectively, while the simulated temperatures (T_{emi_sim}) were 23.25 °C and 22.59 °C. According to Eq. (8), the *RMSD* for the mirror CPC-RC and DCPC-RC modules are 1.93 % and 1.88 %, respectively. These findings confirm that the modelling approach agrees well with experimental outcomes, validating the effectiveness of both the simulation approach and the mathematical model in calculating the emitter temperature for concentrated RC modules and, subsequently, in assessing the maximum net cooling power density (P_{cool}) of the RC module.

3.3. Solar profile angle

Previously, CPC application areas are generally focused on solar collections. To maximize the collection of solar radiation, the tilt angle of the solar energy collection system is adjusted according to the local solar path. However, in the DCPC-RC module, conducting a study on the solar path is also imperative, but the purpose changes to prevent incident sunlight from reaching the RC emitter. This will help mitigate the impact of solar radiation on cooling performance. As the solar azimuth angle (γ) and altitude angle (θ_h) change every moment, the solar position vector is divided into two projection components, i.e., east-west and north-south directions, as shown in Fig. 6. Since the side openings of the DCPC-RC multi-module system are oriented east-west, whereby the projection components in the east-west direction are parallel to the module surface and do not contribute to the solar radiation absorbed by the module. However, the projection component in the north-south direction determines the amount of solar radiation absorbed [42]. In this study, the solar profile angle [43] is used to characterize the projection angle of the southern horizon and the solar position on the north and south meridian planes (ϕ in Fig. 6), ranging from 0° (south horizon) to 180° (northern horizon).

4. Results and discussion

This paper first compares the differences between the ambient temperature and various RC modules' temperature through field

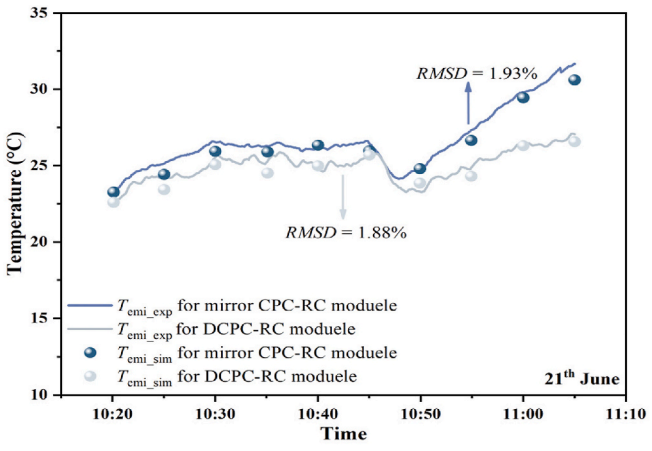

Fig. 5. Simulated and experimental temperatures of the mirror CPC-RC and DCPC-RC modules.

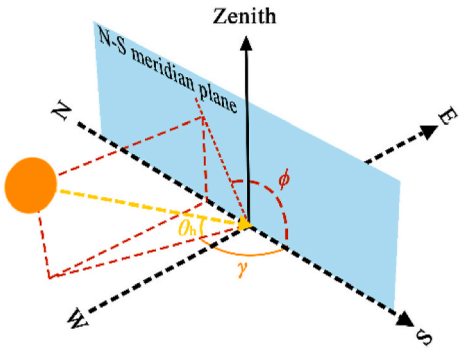

Fig. 6. Definition of solar profile angle (ϕ).

experiments, demonstrating that the DCPC-RC module can mitigate the adverse effects of solar radiation on daytime cooling performance and achieve sub-ambient temperatures. Subsequently, the solar shielding ratio (η) of the DCPC-RC module in different configurations at varying solar profile angles (ϕ) is evaluated, further, to characterize the maximum cooling power density (P_{cool}) for the DCPC-RC module under different configuration parameters. Finally, the concept of hour percentages of ϕ and the solar irradiance distribution in different ϕ are introduced to determine the cooling performance for the DCPC-RC module in cities across various latitudes, ensuring optimal cooling capacity throughout the year. In this section, the DCPC-RC module's surroundings have no obstacle, which is placed horizontally on the brick roof.

4.1. Experimental results

This section discusses experimental results from the night of 25th June and the day of 26th in Nottingham, UK. Fig. 7 (a) illustrates the temperatures of three RC modules alongside ambient temperatures and solar irradiance, while Fig. 7 (b) shows the weather data, including relative humidity and wind speed. Furthermore, Fig. 7 (c) depicts the differences between ambient and RC emitter temperatures. Notably, relative humidity during this period was stable, ranging from 50% to 56 %, and wind speeds remained below 2.5 m/s. These conditions facilitated the RC modules in achieving sub-temperature easily. However, when solar irradiance was present, the flat-RC module, lacking concentrator shading, showed the highest emitter temperatures among the three. For instance, at 19:00, with solar radiation at 318.09 W/m^2, the emitter temperature of the flat-RC module reached 26.73 °C, in contrast to 25.47 °C for the mirror CPC-RC and 24.86 °C for the DCPC-RC modules. As solar radiation diminished to 50 W/m^2, the temperature of the flat-RC module closely matched that of the DCPC-RC module, both dropping to around 16.65 °C by 21:00, while the mirror CPC-RC module exhibited the most pronounced cooling, reaching 15.87 °C at the same time.

When analysing temperature differences between the three RC modules and ambient temperature, it is shown that under solar irradiance, the flat-RC module exhibits the smallest temperature difference, indicating minimal cooling performance. The mirror CPC-RC module, which reflects some solar radiation to the emitter by mirror CPC, shows a slightly larger temperature difference. The DCPC-RC module, due to its distinctive structure, demonstrates the largest temperature differential under these conditions. As solar radiation diminishes, the mirror CPC-RC module achieves the most significant temperature reduction, followed by the flat-RC module, with the DCPC-RC module slightly lagging behind the flat-RC module. Throughout the experiment, the mirror CPC-RC module maintained an average temperature reduction of 3.97 °C from ambient, surpassing the DCPC-RC module, which averaged a 3.37 °C reduction. Finally, the flat-RC module showed the least cooling effect, with a temperature drop of 3.09 °C.

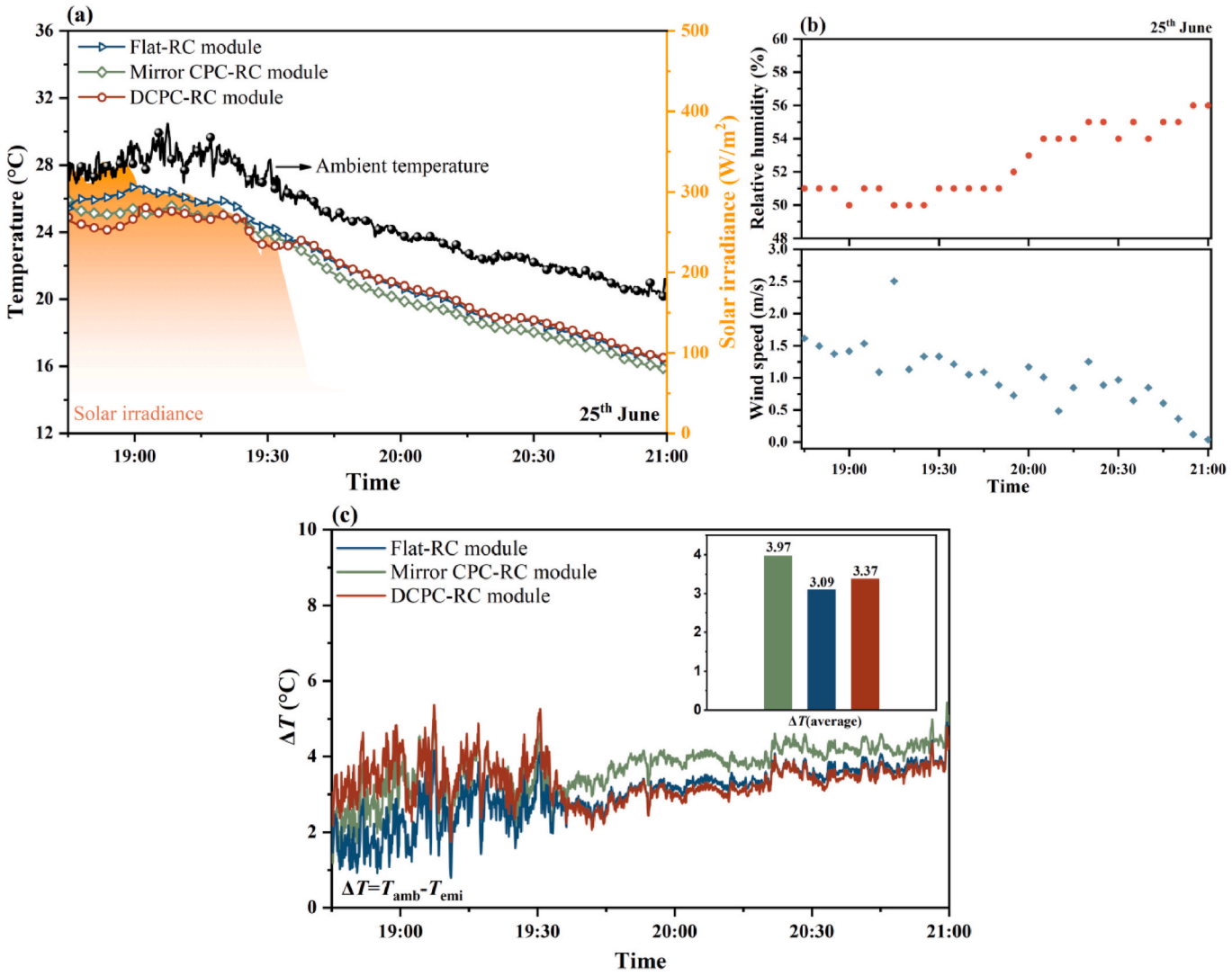

Fig. 7. (a) Measured emitter temperatures of three RC modules alongside ambient temperature and solar irradiance. (b) Weather data in Nottingham, UK on 25th June 2024. (c) Temperature differences (ΔT) between the ambient air and RC emitters.

The experimental results from 26th June are shown in Fig. 8. On this condition, relative humidity was higher than the previous night, ranging from 56 % to 66 %, while wind speeds remained similar. Additionally, solar radiation increased from 715.65 W/m^2 at 10:15–933.40 W/m^2 at 13:15, significantly impacting the cooling performance of the RC modules. Among the three, the flat-RC module was most affected by adverse thermal radiation and could not achieve a sub-ambient temperature. While the mirror CPC-RC module utilizes the CPC as a shield against adverse radiation. However, as the solar altitude angle increased, the solar incident angle fell within the CPC's θ_{max} range, concentrating part of solar radiation on the emitter and causing its temperature to rise above ambient. The DCPC-RC module performed the best cooling effect due to its unique structure, which minimized solar radiation reaching the emitter, consistently maintaining temperatures below ambient. Around 12:35, cloud cover temporarily blocked the solar, leading to a sharp drop in temperatures for three RC modules, most notably for the flat-RC module, which fell from 30.39 to 27.29 °C, while the others experienced smaller declines. These results illustrate the significant impact of solar radiation on RC performance. Furthermore, despite the CPC's shielding capability, in the absence of solar radiation, the CPC-RC module cools slightly slower than the flat-RC module. Fig. 8 (c) displays the temperature difference between the ambient temperature and three RC modules. Notably, apart from the DCPC-RC module, the temperature differences for the other two modules are consistently negative, indicating that their temperatures remain above ambient. At 12:35, cloud cover briefly blocked the sun, causing the temperature differences for all three modules to surge, each exceeding 2 °C. However, once the clouds dispersed, the temperature differences reverted to their previous states. Throughout the experiment, the average emitter temperature of the DCPC-RC module was 0.95 °C below the ambient average, while the mirror CPC-RC and flat-RC modules recorded average temperatures of 0.33 and 0.85 °C above ambient, respectively.

The results from daytime and nighttime experiments highlight the DCPC-RC module's potential for achieving effective all-day RC. However, there is still space for improvement, such as enhancing daytime cooling capacity and nighttime performance. The following sections will explore the cooling power of the DCPC-RC module under various configurations and discuss strategies for further optimizing the module.

4.2. Comparisons and analysis of key performance metrics among three RC modules

To evaluate the overall performance of the DCPC-RC system, three key performance metrics, i.e., solar shielding ratio (η), absorbed solar radiation (P_{sol}) and net cooling power density (P_{cool}), are analysed and compared across three RC modules (DCPC-RC, flat-RC and mirror CPC-

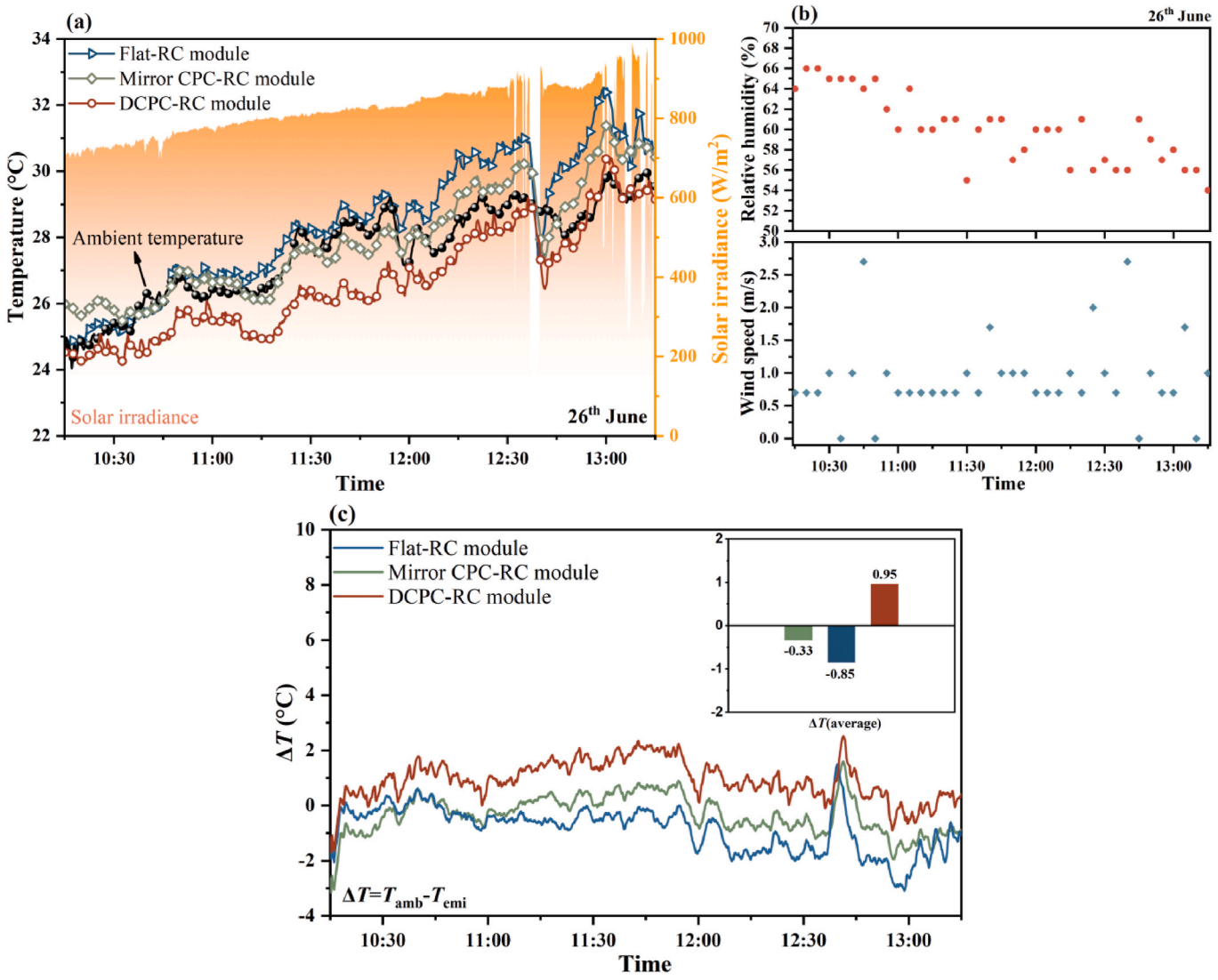

Fig. 8. (a) Measured emitter temperatures of three RC modules alongside ambient temperature and solar irradiance. (b) Weather data in Nottingham, UK on 26th June 2024. (c) Temperature differences (ΔT) between the ambient air and RC emitters.

RC modules) under varying solar profile angles (ϕ).

Specifically, for the flat-RC module, which lacks CPC structure, η remains consistently at 1. In contrast, the η for the two CPC-RC modules: the mirror CPC-RC and DCPC-RC modules, are determined through simulation. Additionally, P_{sol} and P_{cool} for RC modules in Guangzhou, a typical subtropical city, are analysed throughout the day on 21st June to compare their different cooling performance. Weather data for 21st June in Guangzhou, obtained from EnergyPlus [44], is presented in Fig. 9, and key parameter settings for this case are provided in Table 3.

Fig. 10 illustrates the η for two CPC-RC modules at different ϕ. Because the θ_{max} of the mirror CPC is 30°, almost all incoming solar radiation within ±30° of the zenith direction (i.e., ϕ is 60–120°) will be reflected by the mirror CPC to the RC emitter, resulting in η near zero in this range. In this ϕ range, the CPC concentrates solar radiation, adversely affecting RC performance. However, outside the half-acceptance range, the module's η remains at 1, indicating no solar radiation reaches the RC emitter. In contrast, the η curves for the DCPC-RC modules at different ϕ exhibit significant fluctuations, notably when ϕ is 20° or 150°, its η vastly differs from the mirror CPC-RC module. For instance, when ϕ is 20° or 150°, η for the mirror CPC-RC module is 1, while for the DCPC-RC, η is 0.52 or 0.26, respectively. This discrepancy is attributed to the dissimilarity in the material of DCPC wing frameworks.

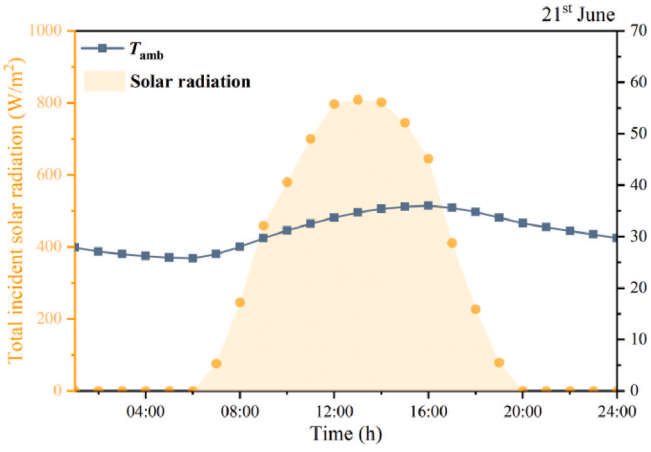

Fig. 9. Hourly total incident solar radiation, ambient and surrounding temperatures on 21st June.

Table 3
Key parameters setting for case studies.

Parameter	Value	Unit
T_{gro_day}	T_{amb}+20 [45]	°C
T_{gro_night}	T_{amb}-5 [46]	°C
ε_{gro}	0.85 [47]	
ε_{emi}	0.95	
α_{emi}	0.1	
α_{cpc}	0	
ρ_{MCPC}	1	
θ_{max} of CPC (DCPC)	30	°
ρ_{TCPC}	1	

Fig. 11 clarifies the incident paths of solar radiation entering the DCPC-RC module at various ϕ. Fig. 11 (a) and (c) illustrate that when ϕ is 20° and 150°, most of the incoming solar radiation, after passing through the transparent wing framework, will be reflected by the adjacent mirror wing framework back to the RC module, eventually reaching the RC emitter, resulting in a lower η at this ϕ. Furthermore, Fig. 11 (b) shows that when ϕ is 100°, the angle falls within the half-acceptance angle range of the DCPC. Consequently, a portion of the solar radiation reaches the RC emitter directly, while the mirror wing framework of the DCPC reflects another portion. This results in η being less than 0.1 at this ϕ. The results show that as ϕ increases, the η for the DCPC-RC module has no obvious regularity in variation, but in the ϕ range of 70–110°, the η for the DCPC is still higher than that of the mirror CPC, indicating its potential to reduce the absorbed P_{sol} by the DCPC-RC module.

Fig. 12 shows the P_{sol} and P_{cool} for three RC modules over a 24-h period on 21st June. It can be seen that during the nighttime, both CPC-RC modules exhibit higher P_{cool}, as the infrared reflectivity of the TIRF is assumed to be the same as that of mirror CPC structure, resulting in similar cooling performance. At 1:00, their P_{cool} reaches 148.35 W/m^2, showing an excellent cooling effect. In contrast, the flat-RC module, lacking a concentrator, shows lower cooling performance, with a P_{cool} 15.5 % lower than the previous two at the same time. However, the situation changes with the presence of solar radiation. The mirror CPC-RC module, due to its concentrating properties, absorbs more solar radiation during the daytime. At noon, its P_{sol} exhibits 120.10 W/m^2, resulting in a P_{cool} of only 40.03 W/m^2. In comparison, the optimized DCPC-RC module, which absorbs only 59.1 W/m^2 of solar radiation at the same time, shows a P_{cool} that is double that of the mirror CPC-RC module, demonstrating superior cooling capability. Meanwhile, the flat-RC module's P_{cool} currently is slightly higher than that of the mirror CPC-RC module, at 54.01 W/m^2, but still lower than the DCPC-RC module. Notably, as previously mentioned, when the solar profile angle is around 100°, the DCPC-RC module's η is minimized, meaning it absorbs more solar radiation. As a result, from 13:00 to 14:00 on 21st June, its P_{cool} is at its lowest for the day, approximately 87.89 W/m^2.

4.3. Effect of spectral selectivity of DCPC-RC module's wing framework on cooling performance

To investigate the impact of DCPC structures with varying spectral characteristics on the overall performance of the RC module, this section analyses and compares the changes in three key parameters of DCPC-RC modules using three different TIRF materials at various solar profile angles (ϕ).

Fig. 13 presents the weighted average transmittance (τ) under the

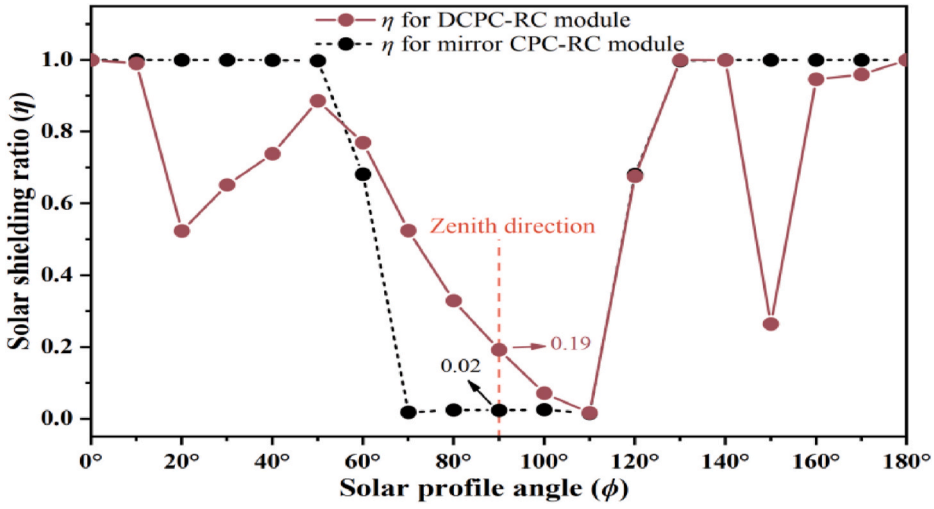

Fig. 10. Solar shielding ratio of different CPC-RC modules under different solar profile angles.

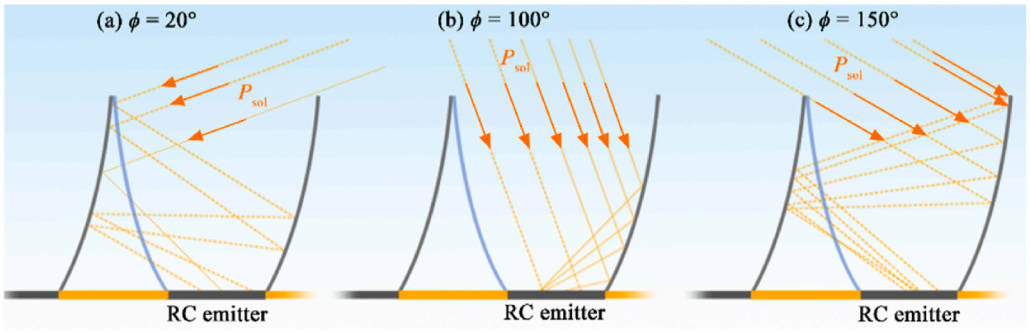

Fig. 11. Traced incoming solar radiation on DCPC-RC multi-module system under different solar profile angles.

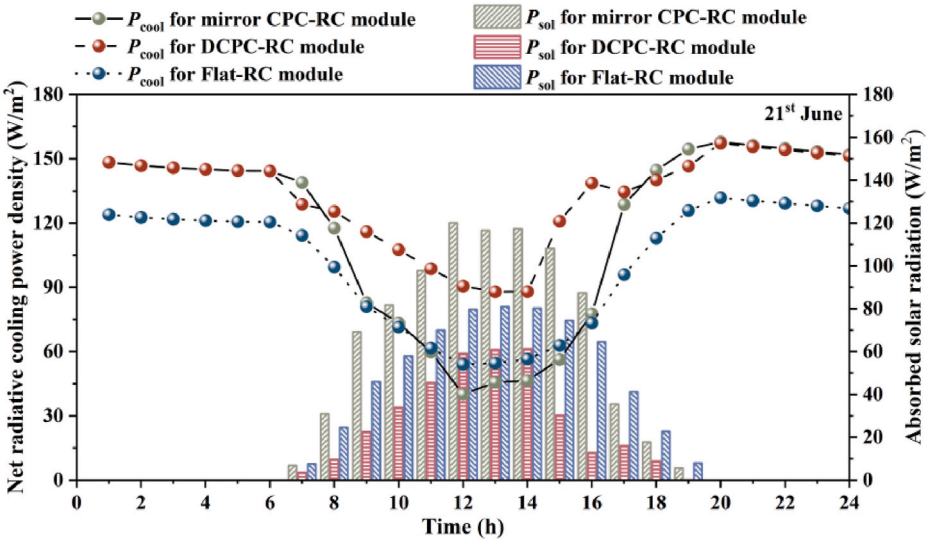

Fig. 12. Absorbed solar radiation and net cooling power density for three RC modules under different solar profile angles.

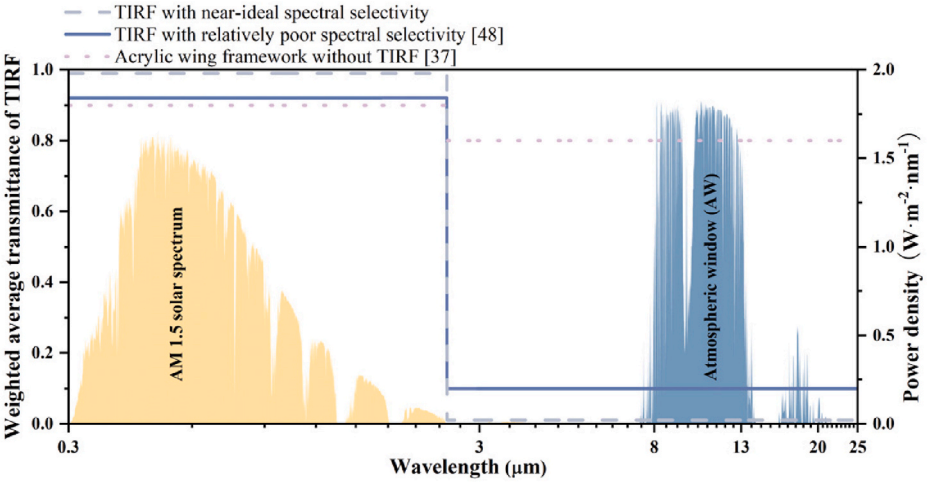

Fig. 13. Weighted average transmittance of DCPC acrylic wing framework with and without TIRF.

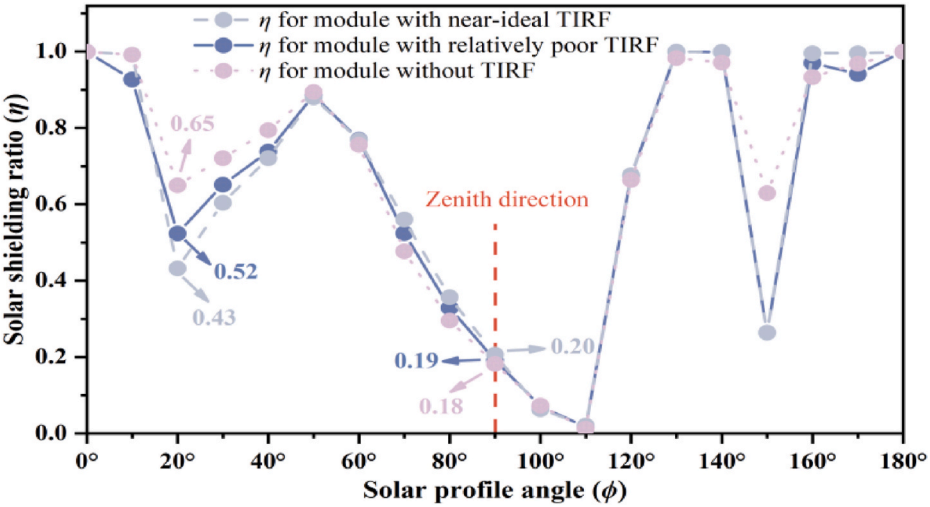

Fig. 14. Solar shielding ratio for the DCPC-RC modules with and without TIRFs under different solar profile angles.

solar spectrum and infrared broadband for two types of TIRFs and the acrylic wing framework without TIRF. The TIRF with near-ideal spectral selectivity (called near-ideal TIRF) is shown to have a τ of 0.99 under the solar spectrum, while its τ at the infrared broadband is extremely low, only 0.01, which is equivalent to an infrared broadband reflectivity of 0.99. The second type is a relatively poor TIRF from Ref. [48] (called relatively poor TIRF), displays a τ of 0.92 under the solar spectrum and 0.1 at the infrared broadband. For comparison, the acrylic wing framework without TIRF (called without TIRF), selected as the control group, exhibits a τ of 0.90 under the solar spectrum and 0.80 at the infrared broadband [37].

Fig. 14 shows the η for the three DCPC-RC modules at different ϕ. The η for all three modules follows similar trends as ϕ changes. At ϕ smaller than 10°, the three modules show the η of 1. But when the ϕ at 20°, a rapid decline in η is observed, with the module with near-ideal TIRF showing the lowest η of 0.43, while the other two modules display slightly higher η of 0.52 and 0.65, respectively. From 20° to 50°, η for all three modules increases as ϕ increases, almost all of them reaching 0.88 at 50°. This indicates that at 50°, only 12 % of the sunlight on the CPC's aperture can reach the RC emitter. However, beyond ϕ of 50°, η for the three modules decreases rapidly and approaches 0 at 110°, suggesting that most of the incident sunlight still reaches the RC emitter when the solar is close to the zenith direction. Fortunately, when ϕ exceeds 110°, a sharp increase in the η for the three modules is seen, particularly for the module with near-ideal TIRF, where η reaches 1 at 130°, which means almost no sunlight reaches the emitter. Nonetheless, at ϕ of 150°, η rebounds as some sunlight is reflected by the mirror wing framework of the adjacent module back to the emitter.

In addition to determining the η for the three DCPC-RC modules at different ϕ, the determination of the ε_{sky} for the three modules is also necessary for characterizing their P_{sky}. The ε_{sky} for the three modules is listed in Table 4. The ε_{sky} for the module with near-ideal TIRF is 0.669, slightly exceeding 0.664 for the module with relatively poor TIRF. This difference is due to the lower τ for the former under the infrared broadband region, which results in almost all the sky thermal radiation being concentrated on the RC emitter by the DCPC. Furthermore, the ε_{sky} for the module without TIRF is 0.627, which is significantly lower than the first two modules. This is also due to its τ under the infrared broadband region being only 0.8, allowing a portion of the sky thermal radiation to pass through the acrylic wing framework.

However, it is noted that a lower ε_{sky} does not necessarily imply a higher P_{cool} for the module. This is because if the infrared broadband reflectivity of the DCPC's acrylic wing framework is not 1, it permits thermal radiation from the solar collector to pass through and reach the RC emitter, as illustrated by the brown line in Fig. 15. Simultaneously, thermal radiation emitted by the emitter can also pass through the acrylic wing framework, either being captured by the collector or returning to the RC emitter, thereby not escaping the system, as depicted by the blue line in Fig. 15.

In this case, the thermal radiation from the emitter finally being trapped in the system (P_{esc}), and the thermal radiation from the solar collector (P_{col}) can be expressed as follows:

$$P_{esc} = \varepsilon_{emi}\sigma T_{emi}^4 \beta_{esc} \quad (9)$$

where β_{esc} is the ratio of the emitted thermal radiation beam that cannot escape from the system to the total hemispheric emitted radiation beam;

$$P_{col} = \alpha_{emi}\varepsilon_{col}\sigma T_{emi}^4 \beta_{col} \quad (10)$$

where ε_{col} is the real material emissivity of the solar collector; β_{col} is the

Table 4
Equivalent sky emissivity for three DCPC-RC modules.

Name	Near-ideal TIRF	Relatively poor TIRF	Without TIRF
ε_{sky}	0.669	0.664	0.627

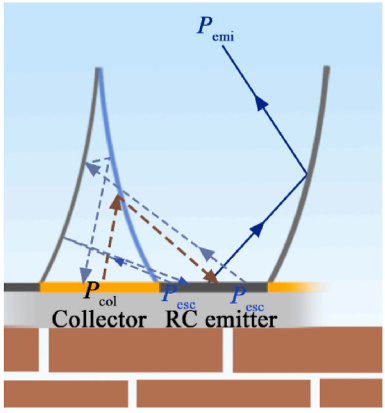

Fig. 15. Schematic diagram of thermal radiation from the solar collector and thermal radiation that cannot escape from the DCPC-RC multi-module system.

ratio of the radiation beam from the system reaching the solar collector to the total hemispheric emitted radiation beam.

Fig. 16 shows the P_{sol} and P_{cool} for the DCPC-RC modules using different TIRFs on 21st June. During the nighttime, the DCPC-RC module with near-ideal TIRF exhibits the highest P_{cool} for the three, close to 150 W/m^2 due to its high infrared reflectivity. In contrast, the DCPC-RC module with relatively poor TIRF, with an infrared emissivity of 0.9, reflects less infrared radiation emitted by the emitter, resulting in a lower P_{cool}. For instance, at 1:00, its P_{cool} is 130.27 W/m^2, which is 12.1 % lower than the DCPC-RC module with near-ideal TIRF. However, the DCPC-RC module without TIRF has a much lower infrared reflectivity of 0.2. Although the infrared thermal radiation passing through the transparent wing framework is partially reflected by the mirror wing framework of the adjacent module, the P_{cool} remains the lowest of the three, 17.2 % lower than the DCPC-RC module with near-ideal TIRF.

During the daytime, the influence of solar radiation causes the P_{cool} for all three DCPC-RC modules to reach its lowest value around noon. This is because the solar transmittance of both TIRF materials and acrylic is above 0.9, with little difference, allowing most solar radiation to pass through the transparent wing framework. However, due to variations in infrared reflectivity, the P_{esc} and P_{col} for the modules differ. It can be seen that the DCPC-RC module without TIRF absorbs the most solar radiation, resulting in the lowest P_{cool}. For example, at noon, the P_{cool} for the DCPC-RC module without TIRF is 99.45 W/m^2, while the modules with near-ideal and relatively poor TIRF show P_{cool} of 119.06 and 105.24 W/m^2, respectively.

By characterizing the maximum net cooling power density of the DCPC-RC modules with TIRFs of varying spectral selectivity or without TIRF, it is observed that the solar radiation absorbed by the three module emitters shows minimal variation, primarily due to the slight differences in solar transmittance among them. The critical factor influencing performance is the reflectivity of the TIRFs in the infrared broadband. Consequently, DCPC-RC modules with near-ideal TIRF demonstrate superior cooling performance.

4.4. Effect of the geographical location of DCPC-RC modules on cooling performance

This section examines the cooling performance of horizontally placed DCPC-RC modules in three typical cities at different latitudes including Guangzhou, Rome, and Nottingham to determine the percentages of hours and solar energy at different ϕ intervals throughout the year. Additionally, the chapter explored the cooling performance of the modules at various ϕ across different cities when the modules are tilted at a specific angle to the anti-sunward side. The transparent wing framework of the DCPC-RC module in this section is covered with near-ideal TIRF. Typical annual weather data for these cities are utilized to

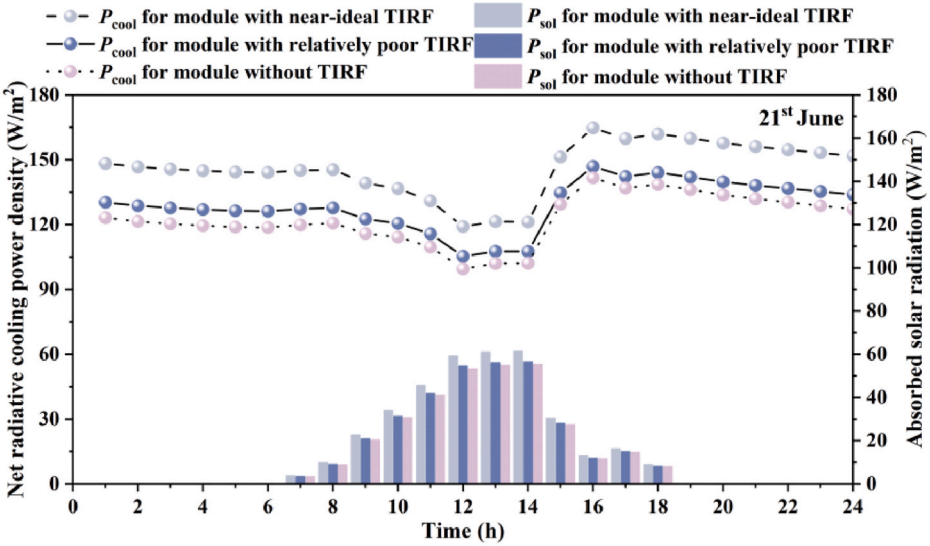

Fig. 16. Absorbed solar radiation and radiative cooling power density for DCPC-RC modules with and without TIRF.

Table 5
Latitudes and solar irradiance of three typical cities [44].

Name	Guangzhou	Rome	Nottingham
Latitudes	23°N	42°N	53°N
Solar Irradiance (kWh/(m²·y))	1256	1642	1018

perform the calculations, with their locations and annual solar irradiance summarized in Table 5.

Fig. 17 shows the number of hours of incident sunlight from different ϕ intervals (in 10° intervals) as a percentage of the total daylight duration throughout the year (ω) for the three cities. Statistical data reveal that Guangzhou experiences 4404 h of total daylight duration throughout the year, while Rome and Nottingham register 4310 and 3850 h respectively. Distinct variations in ω across each ϕ interval are evident among the three cities. For instance, at ϕ ranging from 0–10°, Guangzhou records ω of 1.4 %, whereas Rome and Nottingham exhibit 3.4 % and 6.6 %, respectively. This indicates that higher latitudes experience a greater ω of sunlight coming from the 0°–10° interval annually. Moreover, the ϕ interval corresponding to the maximum ω differs among the cities: Guangzhou's maximum ω exhibits 14.7 % corresponds to ϕ interval of 40~50°, Rome's 14.4 % to ϕ interval of 20°–30°, and Nottingham's highest ω is 17.1 % occurs at 10–20°. Given that solar radiation is highest when ϕ is at the zenith, it is less favourable for RC. By comparing the total ω within the ϕ range of 70°–110°, the challenge of achieving effective RC during the day in each city can be preliminarily assessed. For example, Nottingham's total ω between 70° and 110° is 11.4 %, while Rome and Guangzhou show total ω of 23.3 % and 39.0 %, respectively. This indicates that mitigating the effects of solar radiation on RC modules in Guangzhou is essential for achieving cooling effects.

Fig. 18 shows the solar irradiance distribution in different ϕ intervals, calculated by the total solar irradiance in ϕ intervals relative to the horizontal solar irradiance throughout the year. In Guangzhou, 36.2 % of the solar irradiance distribution originates from the ϕ interval of 40°–60°, while the interval of 80°–100° contributes 28.5 %. This indicates that the highest amount of solar radiation reaching the ground surface in Guangzhou occurs within these two intervals. Therefore, for RC systems, it is crucial to block as much solar radiation from these angles as possible. In Rome, solar irradiance within the 30°–100° range accounts for 75.8 % of the total horizontal irradiance. In contrast, due to its higher latitude, Nottingham experiences a solar irradiance distribution in the 20°–80° of ϕ range, which accounts for 78.2 % of the total

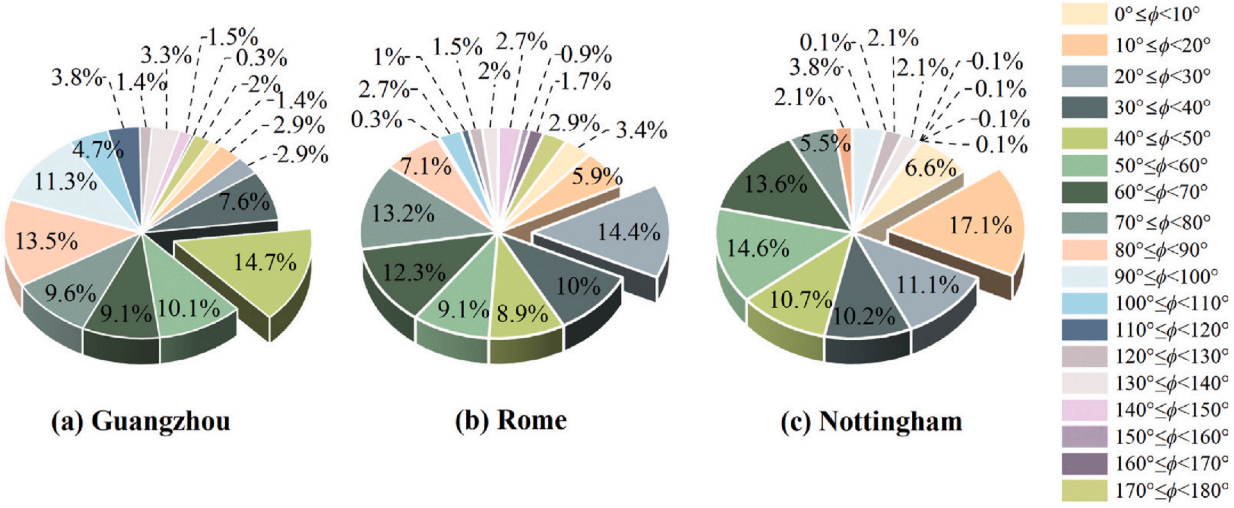

Fig. 17. Hours percentage of different solar profile angle intervals in different cities.

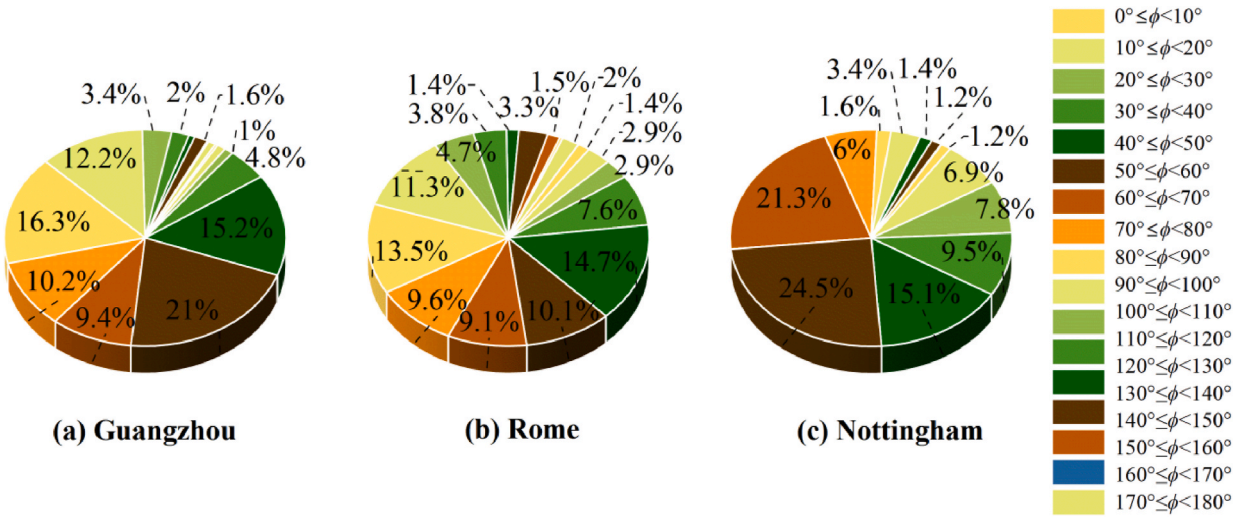

Fig. 18. Percentage of total solar irradiance in different ϕ intervals to the total solar irradiance throughout the year.

horizontal irradiance. The results indicate that, to achieve optimal RC performance throughout the year in different geographic locations, it is essential to further reduce the P_{sol} by tilting the RC module in the ϕ ranges where solar irradiance distribution is most concentrated. Therefore, characterizing the P_{cool} for the DCPC-RC modules tilted at various angles to the anti-sunward side across different ϕ ranges holds significant research value.

To explore the appropriate tilt angle to the anti-sunward side for the RC module in each city, determining the η and ε_{sky} for the tilted modules is first needed. As depicted in Fig. 19, the η for three DCPC-RC modules with different tilt angles at various ϕ shows apparent differences. At ϕ is 0°, the η for three modules is observed to be 1. When ϕ reaches 10°, η of 0.45 is recorded for the module tilted at 0°, while the other two maintain the η of 1. As ϕ further increases, a sharp rise in η to 0.88 (at 50°) followed by a sharp drop to 0 (at 110°) is observed for the module tilted at 0°. The other two modules show a similar general trend, albeit with a delay. Specifically, for the module tilted at 15°, η rises to 0.88 at 70° and drops to 0 at 120°; for the module tilted at 30°, η rises to 0.88 at 80° and falls to 0 at 140°. Furthermore, in the zenith direction, the η for the module tilted at 0° is 0.21, which is 54.6 % and 73.7 % lower than that of the modules tilted at 15° and 30° respectively, indicating that an inclined placement allows the RC module to block more solar radiation at noon. Finally, as η drops to 0 and ϕ further increases, a rapid rise in η to about 1 is observed. However, like the previous subsection, fluctuations in the η for the three modules are experienced after ϕ reaches 150° due to reflections from the metal wing framework of the adjacent module. These fluctuations result in η falling to about 0.2 before rising back to 1.

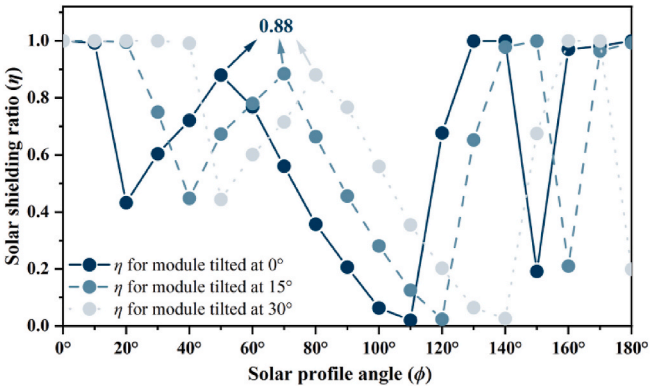

Fig. 19. Solar shielding ratio for the DCPC-RC modules tilted at different angles to the anti-sunward side under different solar profile angles.

Table 6
Equivalent sky emissivity for three ACPC-RC modules tilted at different angles.

Name	Tilted at 0°	Tilted at 15°	Tilted at 30°
ε_{sky}	0.669	0.671	0.675

Table 6 presents the ε_{sky} for the DCPC-RC modules at three different tilt angles. It can be observed that an increase in ε_{sky} with the increase of the tilt angle, rising from 0.669 when the module tilted at 0° to 0.675 when the module tilted at 30°. This is due to the larger sky emissivity at larger zenith angles, and the tilted placement of the module causes the module to receive more sky thermal radiation from the larger zenith angle.

When the module is tilted at different angles, the total global solar radiation in the normal direction of the tilted surface will be different from that when the module is placed horizontally. In this case, the direct solar radiation in the normal direction of the surface tilted at different solar profile angles(ϕ) can be calculated as:

$$G(\phi) = G(\phi)\sin(90-\phi)\cos(-\alpha) + G(\phi)\cos(90-\phi)\cos\gamma\sin(-\alpha) \quad (11)$$

where $G(\phi)$ is direct solar radiation at different ϕ, W/m^2; α is the tilt angle of the module to the anti-sunward side; γ is sun azimuth. Since the solar azimuth angle in this paper is due south, γ is 0°. In this study, the average solar radiation for each angular interval is calculated by statistically analysing the solar radiation from different ϕ intervals over a typical year. This data is then used to characterize the P_{cool} for RC modules under various configurations.

Fig. 20 displays the P_{cool} for DCPC-RC modules tilted at different angles to the anti-sunward side in three cities when the ambient temperature is 30 °C alongside the solar irradiance distribution in different ϕ intervals. It can be observed that in Guangzhou, within the ϕ interval (50–60°), which has the strongest solar energy distribution, the P_{cool} is accordingly lowest across all tilt angles (0°, 15°, and 30°). However, the module tilted at 30° toward the anti-sunward side performs best, achieving a P_{cool} of 127.35 W/m^2, which is 15.2 % higher than the horizontally placed DCPC-RC module. In other ϕ intervals, the larger tilt angle leads to higher P_{gro}, in regions with relatively low solar energy distribution, the P_{cool} for the module tilted at 30° is lower than that tilted at 15°. In Rome, which has the highest solar irradiance among the three cities, tilting the RC module at 30° significantly enhances cooling performance due to improved solar shielding under strong solar irradiance. For example, when ϕ is between 40 and 50°, the P_{cool} reaches 135.24 W/m^2, which is 22.7 % higher than that of the horizontally placed DCPC-RC

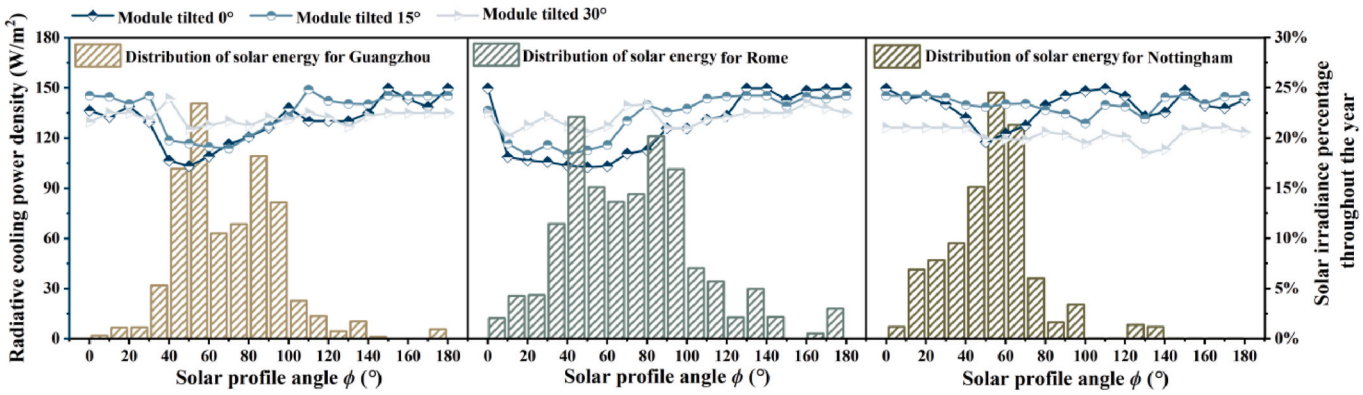

Fig. 20. Cooling performance for DCPC-RC modules tilted at different angles to the anti-sunward side in different cities and the corresponding solar energy distribution throughout the year.

module. Conversely, in Nottingham, which has weak solar irradiance, the tilted configurations provide limited improvement in mitigating solar irradiance. Accordingly, the horizontally placed DCPC-RC module consistently achieves higher cooling performance throughout the year.

5. Conclusions

In this study, a novel RC system based on a dissimilar material CPC (termed as DCPC-RC system) is proposed, and its ability to reduce the absorption of solar radiation by RC emitters is explored. The modelling approach developed in Section 3.2 is applied and validated through experiments conducted in Nottingham, UK. The comparisons show that the simulation results yield good consistency with the experimental data. During the daytime experiments, the DCPC-RC module demonstrates superior performance, with the average emitter temperature being 0.95 °C lower than the ambient temperature and the minimum temperature exceeding 2 °C below the ambient. Additionally, this paper investigates the impact of changing the configurations of the DCPC-RC module on cooling power density (P_{cool}) on a typical summer day in Guangzhou, China. The results led to the following conclusions.

1. When comparing the cooling performance of different RC modules on 21st June, the results indicate that at 1:00, the P_{cool} for two CPC-RC modules reaches 148.35 W/m^2, demonstrating an excellent cooling effect. In contrast, the flat-RC module exhibits lower cooling performance, 15.5 % lower than that of the CPC-RC modules at the same time. However, at noon, both the mirror CPC-RC and flat-RC modules show significantly reduced cooling performance, with P_{cool} of only 40.03 and 54.01 W/m^2, respectively. In comparison, the DCPC-RC module, which absorbs only 59.1 W/m^2 of solar radiation at the same time, achieves a P_{cool} that is nearly double than that of the mirror CPC-RC module.
2. Changing the spectral properties of the transparent wing frameworks of the DCPC-RC module illustrates that different spectral selectivity affects the unfavourable thermal radiation absorbed by the RC emitter. For instance, at noon, the P_{cool} for the DCPC-RC module without TIRF is 99.45 W/m^2, while the modules with near-ideal and relatively poor TIRF show P_{cool} of 119.06 and 105.24 W/m^2, respectively.

In addition, this paper summarizes the distribution of different solar profile angles throughout the year in three cities located at different latitudes, along with the corresponding proportion of solar energy received under each angle. The average solar radiation within each 10° solar profile angle is calculated to characterize the cooling performance of DCPC-RC modules in various cities. This analysis provides new insights for guiding the installation of RC systems in the future, aiming to optimize cooling performance throughout the year.

CRediT authorship contribution statement

Ya Dan: Writing – review & editing, Writing – original draft, Software, Methodology, Investigation, Formal analysis. **Qiliang Wang:** Writing – review & editing, Methodology, Investigation, Formal analysis, Conceptualization. **Mingke Hu:** Writing – review & editing, Formal analysis. **Dongliang Zhao:** Resources, Project administration. **Gang Pei:** Validation, Supervision. **Yuehong Su:** Writing – review & editing, Supervision, Resources, Project administration, Funding acquisition, Conceptualization. **Saffa Riffat:** Writing – review & editing, Resources, Project administration.

Declaration of competing interest

The authors declare that they have no known competing financial interests or personal relationships that could have appeared to influence the work reported in this paper.

Acknowledgements

The authors would like to acknowledge the Engineering and Physical Sciences Research Council (Horizon Europe Guarantee grant number: EP/Y016645/1) and the Royal Society's International Exchange Scheme (grant number: IEC\NSFC\223283) for the financial support to this study.

References

[1] M. Hu, B. Zhao, S. Suhendri, J. Cao, Q. Wang, S. Riffat, R. Yang, Y. Su, G. Pei, Experimental study on a hybrid solar photothermic and radiative cooling collector equipped with a rotatable absorber/emitter plate, Appl. Energy 306 (2022) 118096, https://doi.org/10.1016/j.apenergy.2021.118096.
[2] MdH. Zahir, K. Irshad, M. Shafiullah, N.I. Ibrahim, A.K.M. Kausarul Islam, K. O. Mohaisen, F.A.Al Sulaiman, Challenges of the application of PCMs to achieve zero energy buildings under hot weather conditions: a review, J. Energy Storage 64 (2023) 107156, https://doi.org/10.1016/j.est.2023.107156.
[3] E. Aramendia, P.E. Brockway, P.G. Taylor, J.B. Norman, Exploring the effects of mineral depletion on renewable energy technologies net energy returns, Energy 290 (2024) 130112, https://doi.org/10.1016/j.energy.2023.130112.
[4] Supply – Key World Energy Statistics 2021 – Analysis, IEA (n.d.). https://www.iea.org/reports/key-world-energy-statistics-2021/supply (accessed April 10, 2024).
[5] Q. Ma, Y. Zhang, G. Wu, Q. Yang, Y. Yuan, R. Cheng, Y. Tong, H. Fang, Photovoltaic/spectrum performance analysis of a multifunctional solid spectral splitting covering for passive solar greenhouse roof, Energy Convers. Manag. 251 (2022) 114955, https://doi.org/10.1016/j.enconman.2021.114955.
[6] K. Irshad, M.H. Zahir, M.S. Shaik, A. Ali, Buildings' heating and cooling load prediction for hot arid climates: a novel intelligent data-driven approach, Buildings 12 (2022) 1677, https://doi.org/10.3390/buildings12101677.
[7] Q. Gong, L. Lu, J. Chen, Design and performance investigation of a novel self-adaptive radiative cooling module for thermal regulation in buildings, Appl. Energy 352 (2023) 121928, https://doi.org/10.1016/j.apenergy.2023.121928.
[8] B. Zhao, K. Lu, M. Hu, K. Wang, D. Gao, K. Chen, Q. Xuan, G. Pei, Sub-ambient daytime radiative cooling based on continuous sunlight blocking, Sol. Energy

Mater. Sol. Cell. 245 (2022) 111854, https://doi.org/10.1016/j.solmat.2022.111854.
[9] H. Ju, S. Lei, F. Wang, D. Yang, J. Ou, A. Amirfazli, Daytime radiative cooling performance and building energy consumption simulation of superhydrophobic calcined kaolin/poly(vinylidene fluoride-co-hexafluoropropylene) coatings, Energy Build. 292 (2023) 113184, https://doi.org/10.1016/j.enbuild.2023.113184.
[10] J. Chen, L. Lu, Development of radiative cooling and its integration with buildings: a comprehensive review, Sol. Energy 212 (2020) 125–151, https://doi.org/10.1016/j.solener.2020.10.013.
[11] S. Suhendri, M. Hu, Y. Su, J. Darkwa, S. Riffat, Performance evaluation of combined solar chimney and radiative cooling ventilation, Build. Environ. 209 (2022) 108686, https://doi.org/10.1016/j.buildenv.2021.108686.
[12] D. Zhao, A. Aili, Y. Zhai, J. Lu, D. Kidd, G. Tan, X. Yin, R. Yang, Subambient cooling of water: toward real-world applications of daytime radiative cooling, Joule 3 (2019) 111–123, https://doi.org/10.1016/j.joule.2018.10.006.
[13] D. Zhao, A. Aili, Y. Zhai, S. Xu, G. Tan, X. Yin, R. Yang, Radiative sky cooling: fundamental principles, materials, and applications, Appl. Phys. Rev. 6 (2019) 021306, https://doi.org/10.1063/1.5087281.
[14] B. Jamil, K. Irshad, A. Algahtani, S. Islam, M.A. Ali, A. Shahab, On the calibration and applicability of global solar radiation models based on temperature extremities in India, Environ. Prog. Sustain. Energy 39 (2020) 13236, https://doi.org/10.1002/ep.13236.
[15] T. Wang, Y. Wu, L. Shi, X. Hu, M. Chen, L. Wu, A structural polymer for highly efficient all-day passive radiative cooling, Nat. Commun. 12 (2021) 365, https://doi.org/10.1038/s41467-020-20646-7.
[16] A.P. Raman, M.A. Anoma, L. Zhu, E. Rephaeli, S. Fan, Passive radiative cooling below ambient air temperature under direct sunlight, Nature 515 (2014) 540–544, https://doi.org/10.1038/nature13883.
[17] Y. Zhai, Y. Ma, S.N. David, D. Zhao, R. Lou, G. Tan, R. Yang, X. Yin, Scalable-manufactured randomized glass-polymer hybrid metamaterial for daytime radiative cooling, Science 355 (2017) 1062–1066, https://doi.org/10.1126/science.aai7899.
[18] A.A. Alshammari, E.M. Salilih, E. Almatrafi, M. Rady, Polymeric coatings for passive radiative cooling of PV modules in hot and humid weather: design, optimization, and performance evaluation, Case Stud. Therm. Eng. 57 (2024) 104341, https://doi.org/10.1016/j.csite.2024.104341.
[19] S. Zhao, B. Da, F. Peng, B. Hu, C. Gao, K. Dai, G. Zheng, C. Liu, C. Shen, Facilely fabricated polyethylene film composed of directional microfibrils for passive radiative cooling, Polymer 299 (2024) 126979, https://doi.org/10.1016/j.polymer.2024.126979.
[20] Y. Wu, B. Liu, R. Zhang, T. Yu, M. Pu, X. Li, X. Ma, Y. Guo, X. Luo, Temperature-adaptive porous polymer radiative cooling coatings for all-season thermal management and annual energy-saving, Energy Build. 296 (2023) 113423, https://doi.org/10.1016/j.enbuild.2023.113423.
[21] H. Sun, F. Tang, Q. Chen, L. Xia, C. Guo, H. Liu, X. Zhao, D. Zhao, L. Huang, J. Li, L. Chen, A recyclable, up-scalable and eco-friendly radiative cooling material for all-day sub-ambient comfort, Chem. Eng. J. 455 (2023) 139786, https://doi.org/10.1016/j.cej.2022.139786.
[22] R. Yang, D. Niu, J.H. Pu, G.H. Tang, X. Wang, M. Du, Passive all-day freshwater harvesting through a transparent radiative cooling film, Appl. Energy 325 (2022) 119801, https://doi.org/10.1016/j.apenergy.2022.119801.
[23] I. Haechler, H. Park, G. Schnoering, T. Gulich, M. Rohner, A. Tripathy, A. Milionis, T.M. Schutzius, D. Poulikakos, Exploiting radiative cooling for uninterrupted 24-hour water harvesting from the atmosphere, Sci. Adv. 7 (2021) eabf3978, https://doi.org/10.1126/sciadv.abf3978.
[24] Z. Chen, L. Zhu, A. Raman, S. Fan, Radiative cooling to deep sub-freezing temperatures through a 24-h day–night cycle, Nat. Commun. 7 (2016) 13729, https://doi.org/10.1038/ncomms13729.
[25] A. Pirvaram, T. Cooper, S.N. Leung, P.G. O'Brien, A comprehensive study on using underside infrared reflectors to enhance the performance of radiative cooling structures, Energy Convers. Manag. 304 (2024) 118180, https://doi.org/10.1016/j.enconman.2024.118180.
[26] S. Lv, X. Sun, B. Zhang, Y. Lai, J. Yang, Research on the influence and optimization of sunshade effect on radiative cooling performance, Energy (2024) 131172, https://doi.org/10.1016/j.energy.2024.131172.
[27] J. Peoples, Y.-W. Hung, X. Li, D. Gallagher, N. Fruehe, M. Pottschmidt, C. Breseman, C. Adams, A. Yuksel, J. Braun, W.T. Horton, X. Ruan, Concentrated radiative cooling, Appl. Energy 310 (2022) 118368, https://doi.org/10.1016/j.apenergy.2021.118368.
[28] M. Dong, L. Zhu, B. Jiang, S. Fan, Z. Chen, Concentrated radiative cooling and its constraint from reciprocity, Opt. Express 30 (2022) 275, https://doi.org/10.1364/OE.445544.
[29] L. Zhou, H. Song, N. Zhang, J. Rada, M. Singer, H. Zhang, B.S. Ooi, Z. Yu, Q. Gan, Hybrid concentrated radiative cooling and solar heating in a single system, Cell Reports Physical Science 2 (2021) 100338, https://doi.org/10.1016/j.xcrp.2021.100338.
[30] Q. Wang, Y. Dan, S. Riffat, H. Yang, Y. Su, M. Hu, Harvesting energy from the sun and space: a versatile collector for simultaneous production of electricity, heat, and cold energy, The Innovation Energy 1 (2024) 100013, https://doi.org/10.59717/j.xinn-energy.2024.100013.
[31] E. du M. van Voorthuysen, R. Roes, Blue sky cooling for parabolic trough plants, Energy Proc. 49 (2014) 71–79, https://doi.org/10.1016/j.egypro.2014.03.008.
[32] Y. Dan, M. Hu, S. Suhendri, Y. Su, S. Riffat, Harnessing the characteristic of compound parabolic concentrators for directional concentration of emitted thermal radiation and solar shielding in building-integrated radiative cooling, Energy Build. 307 (2024) 113922, https://doi.org/10.1016/j.enbuild.2024.113922.
[33] Y. Dan, M. Hu, Q. Wang, Y. Su, S. Riffat, Comprehensive evaluation of integrating radiative sky cooling with compound parabolic concentrator for cooling flux amplifying, Energy 312 (2024) 133673, https://doi.org/10.1016/j.energy.2024.133673.
[34] M.A. Khan, N. Islam, M. Abdul Mateen Khan, K. Irshad, M. Hanzala, A. Ali Pasha, M. Mursaleen, Experimental and simulation analysis of grid-connected rooftop photovoltaic system for a large-scale facility, Sustain. Energy Technol. Assessments 53 (2022) 102773, https://doi.org/10.1016/j.seta.2022.102773.
[35] Y. Dan, M. Hu, Y. Su, S. Riffat, A generalized modelling approach to performance analysis of radiative sky cooling with complicated configurations and external environments, Renew. Energy (2024) 121729, https://doi.org/10.1016/j.renene.2024.121729.
[36] ITO-Coated PET Film, (n.d.). https://www.thorlabs.com (accessed July 9, 2024).
[37] M. Hu, Suhendri, B. Zhao, X. Ao, J. Cao, Q. Wang, S. Riffat, Y. Su, G. Pei, Effect of the spectrally selective features of the cover and emitter combination on radiative cooling performance, Energy and Built Environment 2 (2021) 251–259, https://doi.org/10.1016/j.enbenv.2020.06.008.
[38] B. Bhatia, A. Leroy, Y. Shen, L. Zhao, M. Gianello, D. Li, T. Gu, J. Hu, M. Soljačić, E. N. Wang, Passive directional sub-ambient daytime radiative cooling, Nat. Commun. 9 (2018) 5001, https://doi.org/10.1038/s41467-018-07293-9.
[39] L. Evangelisti, C. Guattari, F. Asdrubali, On the sky temperature models and their influence on buildings energy performance: a critical review, Energy Build. 183 (2019) 607–625, https://doi.org/10.1016/j.enbuild.2018.11.037.
[40] Optical Design Software | Photopia | Photopia Optical Design Software, (n.d.). https://www.ltioptics.com/en/optical-design-software-photopia.html (accessed January 31, 2023).
[41] Y. Zhang, M. Hu, Z. Chen, Y. Su, S. Riffat, Performance study of a thermochemical energy storage reactor embedded with a microchannel tube heat exchanger for water heating, J. Energy Storage 78 (2024) 110043, https://doi.org/10.1016/j.est.2023.110043.
[42] X. Yu, Y. Su, A discussion of inner south projection angle for performance analysis of dielectric compound parabolic concentrator, Sol. Energy 113 (2015) 101–113, https://doi.org/10.1016/j.solener.2014.12.024.
[43] B. Müller, T. Reis, A. Driesse, C. Reise, MAXIMIZING THE YIELD OF LARGE PV POWER PLANTS: WHAT CAN WE LEARN FROM MONITORING AND SIMULATION?, 2012.
[44] EnergyPlus, (n.d.). https://energyplus.net/(accessed August 5, 2022).
[45] K. Niachou, I. Livada, M. Santamouris, Experimental study of temperature and airflow distribution inside an urban street canyon during hot summer weather conditions. Part II: airflow analysis, Build. Environ. 43 (2008) 1393–1403, https://doi.org/10.1016/j.buildenv.2007.01.040.
[46] A. Synnefa, M. Santamouris, I. Livada, A study of the thermal performance of reflective coatings for the urban environment, Sol. Energy 80 (2006) 968–981, https://doi.org/10.1016/j.solener.2005.08.005.
[47] J. Torres-Quezada, A. Isalgué, H. Coch, Impact of solar reflectivity and infrared emissivity on the thermal performance of metal and concrete roofs in cloudy warm-humid climate, Frontiers of Architectural Research 13 (2024) 842–857, https://doi.org/10.1016/j.foar.2024.03.003.
[48] K.P. Sibin, N. Selvakumar, A. Kumar, A. Dey, N. Sridhara, H.D. Shashikala, A. K. Sharma, H.C. Barshilia, Design and development of ITO/Ag/ITO spectral beam splitter coating for photovoltaic-thermoelectric hybrid systems, Sol. Energy 141 (2017) 118–126, https://doi.org/10.1016/j.solener.2016.11.027.